

University of Wollongong

Research Online

Australian Institute for Innovative Materials -
Papers

Australian Institute for Innovative Materials

1-1-2019

Sheath-run artificial muscles

Jiuke Mu

University of Texas at Dallas

Monica Jung de Andrade

University of Texas at Dallas

Shaoli Fang

University of Texas at Dallas

Xuemin Wang

University of Texas at Dallas, Georgia Southern University

Enlai Gao

Wuhan University, University of Texas at Dallas

See next page for additional authors

Follow this and additional works at: <https://ro.uow.edu.au/aiimpapers>



Part of the [Engineering Commons](#), and the [Physical Sciences and Mathematics Commons](#)

Recommended Citation

Mu, Jiuke; de Andrade, Monica Jung; Fang, Shaoli; Wang, Xuemin; Gao, Enlai; Li, Na; Kim, Shi Hyeong; Wang, Hongzhi; Hou, Chengyi; Zhang, Qinghong; Zhu, Meifang; Qian, Dong; Lu, Hongbing; Kongahage, Dharshika; Talebian, Sepehr; Foroughi, Javad; Spinks, Geoffrey M.; Kim, Hyun; Ware, Taylor H.; Sim, Hyeon Jun; Lee, Dong Yeop; Jang, Yongwoo; Kim, Seon Jeong; and Baughman, Ray H., "Sheath-run artificial muscles" (2019). *Australian Institute for Innovative Materials - Papers*. 3746.
<https://ro.uow.edu.au/aiimpapers/3746>

Research Online is the open access institutional repository for the University of Wollongong. For further information contact the UOW Library: research-pubs@uow.edu.au

Sheath-run artificial muscles

Abstract

Although guest-filled carbon nanotube yarns provide record performance as torsional and tensile artificial muscles, they are expensive, and only part of the muscle effectively contributes to actuation. We describe a muscle type that provides higher performance, in which the guest that drives actuation is a sheath on a twisted or coiled core that can be an inexpensive yarn. This change from guest-filled to sheath-run artificial muscles increases the maximum work capacity by factors of 1.70 to 2.15 for tensile muscles driven electrothermally or by vapor absorption. A sheath-run electrochemical muscle generates 1.98 watts per gram of average contractile power—40 times that for human muscle and 9.0 times that of the highest power alternative electrochemical muscle. Theory predicts the observed performance advantages of sheath-run muscles.

Disciplines

Engineering | Physical Sciences and Mathematics

Publication Details

Mu, J., de Andrade, M. Jung., Fang, S., Wang, X., Gao, E., Li, N., Kim, S. Hyeong., Wang, H., Hou, C., Zhang, Q., Zhu, M., Qian, D., Lu, H., Kongahage, D., Talebian, S., Foroughi, J., Spinks, G., Kim, H., Ware, T. H., Sim, H. Jun., Lee, D. Yeop., Jang, Y., Kim, S. Jeong. & Baughman, R. H. (2019). Sheath-run artificial muscles. *Science*, 365 (6449), 150-155.

Authors

Jiuke Mu, Monica Jung de Andrade, Shaoli Fang, Xuemin Wang, Enlai Gao, Na Li, Shi Hyeong Kim, Hongzhi Wang, Chengyi Hou, Qinghong Zhang, Meifang Zhu, Dong Qian, Hongbing Lu, Dharshika Kongahage, Sepehr Talebian, Javad Foroughi, Geoffrey M. Spinks, Hyun Kim, Taylor H. Ware, Hyeon Jun Sim, Dong Yeop Lee, Yongwoo Jang, Seon Jeong Kim, and Ray H. Baughman

Sheath-Run Artificial Muscles

Jiuke Mu¹, Mônica Jung de Andrade¹, Shaoli Fang¹, Xuemin Wang³, Enlai Gao¹, Na Li¹, Shi Hyeong Kim¹, Hongzhi Wang², Chengyi Hou², Qinghong Zhang², Meifang Zhu², Dong Qian³, Hongbing Lu³, Dharshika Kongahage⁴, Sepehr Talebian⁴, Javad Foroughi⁴, Geoffrey Spinks⁴, Hyun Kims⁵, Taylor H. Ware⁵, Hyeon Jun Sim⁶, Dong Yeop Lee⁶, Yongwoo Jang⁶, Seon Jeong Kim⁶, Ray H. Baughman^{1*}

Abstract

While guest-filled carbon nanotube yarns provide record performance as torsional and tensile artificial muscles, they are expensive and only part of the muscle effectively contributes to actuation. We describe a muscle type providing higher performance, wherein the guest that drives actuation is a sheath on a twisted or coiled core that can be an inexpensive yarn. This change from guest-filled to sheath-run artificial muscles increases the maximum work capacity by factors of 1.70 to 2.15 for tensile muscles driven electrothermally or by vapor absorption. A sheath-run electrochemical muscle generates 1.98 W/g of average contractile power - 40 times that for human muscle and 9.0 times that of the highest power alternative electrochemical muscle. Theory predicts the observed performance advantages of sheath-run muscles.

¹Alan G. MacDiarmid NanoTech Institute, The University of Texas at Dallas, Richardson, TX 75080, USA.

²State Key Laboratory for Modification of Chemical Fibers and Polymer Materials, College of Material Science and Engineering, Donghua University, Shanghai 201620, China.

³Department of Mechanical Engineering, The University of Texas at Dallas, Richardson, TX 75080, USA.

⁴Intelligent Polymer Research Institute, Australian Institute for Innovative Materials, University of Wollongong, Wollongong, New South Wales 2522, Australia.

⁵Department of Bioengineering, The University of Texas at Dallas, Richardson, TX 75080, USA.

⁶Center for Self-Powered Actuation, Department of Biomedical Engineering, Hanyang University, Seoul 04763, South Korea.

*Corresponding author: ray.baughman@utdallas.edu

One Sentence Summary: A described new structure enables inexpensive yarn muscles, where a sheath on a coiled yarn drives actuation that provides much higher work-per-cycle and power densities than for previous muscles.

Remarkable performance has been obtained for tensile and torsional carbon nanotube hybrid yarn muscles (1-5), whose actuation is driven by the volume change of a guest within a twisted or coiled carbon nanotube yarn. During thermally-powered contraction, coiled hybrid muscles can deliver 29 times the work as the same weight human muscle (1). Changing the structural relationship between guest and host will provide major performance increases and the ability to replace expensive carbon nanotube yarn with cheap commercialized yarns.

Carbon nanotube (CNT) hybrid yarn artificial muscles (HYAMs) can be made by inserting twist, or twist and coiling, into a guest-filled CNT yarn. Muscles that are twisted (but not coiled), called twisted muscles, are mainly useful for torsional actuation. High inserted twist results in coiled muscles that can deliver larger strokes than human muscles (1).

Polymer fiber and yarn muscles are known (6-10, 11) that operate similarly to CNT HYAMs: muscle volume expansion drives muscle untwist, which produces both torsional and tensile actuation. These thermally driven polymer muscles are cheap, since they can be made by inserting extreme twist into fishing line or sewing thread. Other twisted or coiled materials have been exploited as fiber-like muscles, such as graphene oxide fiber (12), shape memory polymer fiber or metal alloy yarn (13, 14), cotton yarn composites (15), carbon fiber/polydimethylsiloxane yarn (16), neat CNT yarns (1, 17-20), and spider-silk dragline (21). CNT HYAMs are especially useful since guest choice results in muscles driven thermally (1, 4), electrochemically (22, 23), or by absorption (2, 3, 24).

The challenge is to develop a fundamentally new host-guest structure that eliminates the liabilities of CNT HYAMs. First, the ability of guest expansion to drive yarn untwist depends on the yarn's bias angle (the angle between the yarn length and the nanotube direction). Since this angle decreases to zero on going from yarn surface to yarn center, the input energy delivered to guest near yarn center is not effectively utilized. Second, muscle mechanical power is limited by the chemical or thermal transport times to access yarn volume.

We here describe a new muscle structure that addresses each of these problems. Rather than infiltrating a volume-changing yarn guest within a yarn, like for a HYAM, this guest is coated as a yarn sheath. Since the dimensional and modulus changes of this sheath drive actuation, we call the resulting actuators "sheath-run artificial muscles" (SRAMs).

Fabrication of sheath-run artificial muscles

CNTs were drawn as a sheet from a CNT forest and twisted into the Archimedian yarn (25, 26, fig. S1) used as muscle core. SRAMs were fabricated (Fig. 1A) by drawing a vertically-suspended, torsionally-tethered twisted yarn through a large droplet of polymer solution multiple times to achieve the targeted sheath thickness of dried polymer. The solvent used was chosen to avoid polymer infiltration into the twist-densified core yarn and provide a sharp interface between sheath and core (Fig. 1C, fig. S2A, fig. S3 and figs. S7C-F). Scanning electron microscope (SEM) measurements provided the sheath/core ratio (SCR, the ratio of sheath thickness to the interior yarn diameter). To demonstrate that CNT yarns can be replaced by inexpensive yarns, we evaluated commercial nylon 6, silk, and bamboo yarns as the muscle core, as well as electrospun polyacrylonitrile (PAN) nanofibers.

The nomenclature used for a sheath X on a yarn core Y of a SRAM or an X guest inside a HYAM yarn Y is X@Y. Hence, PEO-SO₃@CNT denotes a PEO-SO₃ guest and a CNT yarn host, where PEO-SO₃ is a blend of poly(ethylene oxide) and a co-polymer of tetrafluoroethylene and sulfonyl fluoride vinyl ether (26). Figure S7 shows the yarn-bias-angle dependence of the minimum SCR needed to prevent sheath cracking for a PEO-SO₃@CNT yarn, and that this ratio approximately maximizes torsional stroke for the high targeted yarn bias angle. For comparative studies, the guest/host weight ratio was essentially the same for the SRAM and HYAM and the same mechanical load was applied during twist insertion. HYAMs were made using the above droplet method by adding polymer solution to a low-twist-yarn, partially drying the solution to a gel-like state, and then adding additional twist to equal that of the SRAM. If the guest/host weight ratio is too high for a HYAM (26), guest will extrude from the host yarn during twist insertion (fig. S12B).

“Self-coiled” yarn was fabricated by inserting further twist, while the guest was in the gel state (Fig. 1B). To increase yarn stroke by increasing the spring index, twisted yarns or self-coiled yarns (Fig. 1D, E) were coiled or supercoiled by wrapping around a mandrel. Afterwards, the coiled yarn was thermally annealed (26). When describing a muscle, the diameter is for the dry, twisted muscle before coiling. Unless otherwise described, gravimetric work and power densities are normalized to the weight of the dry muscle. The spring index is the ratio of the

difference in outer coil diameter and the fiber diameter to the fiber diameter, where a fiber's diameter is its width in its largest lateral dimension.

Torsional actuation of twisted muscles powered by sorption

Figure 2A illustrates torsional actuation of a one-end-tethered SRAM. Unless otherwise noted, an equilibrium vapor pressure was delivered to muscles in flowing dry air and then removed under vacuum, using the glass tube system of Fig. 2B. For performance comparisons, a 60-mg-weight paddle at yarn end, with $0.28 \text{ kg}\cdot\text{mm}^2$ moment of inertia, was used to characterize torsional rotation angle and speed. Also, the SRAMs and HYAMs were made from identical yarn, contained the same inserted twist, and had nearly the same host/guest weight ratio.

Figure 2B compares the time dependence of paddle rotation and speed for a PEO-SO₃@CNT SRAM and HYAM and a pristine CNT muscle that are undergoing one complete reversible cycle of ethanol-vapor-powered actuation. The peak stroke and peak rotation speed for the SRAM ($143^\circ/\text{mm}$ and 507 rpm) are about twice that for the HYAM ($76^\circ/\text{mm}$ and 254 rpm), and much larger than for the pristine yarn ($4.7^\circ/\text{mm}$ and 36 rpm). Steady-state measurements of torsional stroke versus weight-percent (wt %) ethanol in the muscles (Fig. 2C) show that the ratio of torsional strokes for a PEO-SO₃@CNT SRAM to a PEO-SO₃@CNT HYAM peaks at 6.7 for 4.1 wt % ethanol, and then gradually decreases to 1.7 for 17.5 wt % ethanol. The small hysteresis in torsional strokes for the SRAM and HYAM means that both could reliably open and close valves in response to absorbed vapor. However, the torsional stroke of the SRAM is much more sensitive to the amount of absorbed ethanol than the HYAM.

Figure 2D shows that PEO-SO₃@CNT SRAMs and HYAMs reversibly actuate over 3000 cycles of ethanol absorption and desorption, despite the absence of tethering. This reversibility results since the guest acts as a torsional return spring. In contrast, the torsional stroke of the pristine yarn rapidly decreases from $27^\circ/\text{mm}$ for the first cycle to about $4.7^\circ/\text{mm}$ on the 27th cycle, thereafter stabilizing at this value for the next ~3000 cycles.

Our theoretical model (26) predicts the dependence of torsional stroke on the SCR by using the torque balance between sheath and core, before and after actuation. This analysis captures the two primary mechanistic contributions to SRAM torsional actuation: sheath swelling and sheath softening, which combine to partially release elastically-stored torsional

energy in the core yarn. Fig. 2E compares the observed and predicted dependence of torsional stroke on SCR for an ethanol-driven PEO-SO₃@CNT SRAM made from a 42°-bias-angle yarn. The maximum torsional stroke (143°/mm) occurs for a SCR of 0.14, which agrees with the predicted 151°/mm stroke maximum for a SCR of 0.15. A much lower SCR cannot maintain the initially inserted twist before actuation and a much higher SCR ratio hinders twist release during actuation. Figure S6 shows that the torsional stroke is near maximum for yarn bias angles from 38° to 43°, for a PEO-SO₃@CNT SRAM having a sheath/core weight ratio of 0.53.

Torsional stroke is sensitive to vapor type (fig. S8) and the sheath's ability to swell and soften by vapor absorption. Since ethanol produces a much larger equilibrium volume expansion in PEO-SO₃ (16.7%) than in polyvinyl alcohol (PVA, 1.3%) or nylon 6 (0.5%) (fig. S5A), the torsional stroke of a CNT core SRAM was much larger for a PEO-SO₃ sheath (143°/mm) than for PVA (22°/mm) or nylon 6 sheaths (11°/mm) (fig. S5B).

High performance resulted for ethanol-powered torsional SRAMs in which the expensive CNT yarn was replaced by a silk or electrospun PAN yarn (Fig. 2F, fig. S2B). The bias angles of these SRAMs (30° and 18°, respectively) are lower than for the CNT yarn core SRAM (42°), since higher twist broke the yarns. The lower bias angles and larger diameters of the PAN and silk core yarns provided smaller equilibrium torsional strokes (123 and 70°/mm, respectively) than for the PEO-SO₃@CNT SRAM (143°/mm). However, using the invariance of the product of torsional stroke and yarn diameter when the yarn's bias angle is constant (*I*) and results in fig. S6 for the bias-angle-dependence of torsional stroke for a PEO-SO₃@CNT SRAM, the torsional strokes of a PEO-SO₃@PAN SRAM and a PEO-SO₃@silk SRAM are predicted to be close to those for PEO-SO₃@CNT SRAMs having the same core bias angle and diameter (26).

All measurements show that a SRAM has important performance advantages over the corresponding HYAM as a torsional actuator. The ratios of peak torsional speed of the SRAM to that of the corresponding HYAM are nearly the same for PEO-SO₃@CNT (1.75), PEO-SO₃@silk (1.74), and PEO-SO₃@PAN (1.79) muscles powered by ethanol vapor, and close to that for water-vapor-powered nylon6@CNT muscles (1.86) (Fig. 2B, F and figs. S2, S9). However, greater variation arises in the ratios of peak stroke for the SRAM to that of the HYAM (1.86, 1.67, 1.36, 1.63, respectively, for the above).

Tensile actuation of coiled muscles powered thermally or by sorption

By adding sufficient additional twist to the muscles used for torsional actuation, fully-coiled yarn muscles result that provide large strokes. By comparing the performance of coiled muscles made from yarns with nearly the same host and guest weight per yarn length, we will demonstrate the increases in stroke, stroke rate, contractile work, and contractile power resulting from transitioning from a HYAM to a SRAM.

The torsional rotor was replaced by a heavy, non-rotating weight when changing from torsional to tensile actuation. Allowing weight rotation decreases tensile contraction (fig. S10), since yarn untwist increases muscle length. When ethanol-vapor-driven, a PEO-SO₃@CNT SRAM delivered a higher stroke for all loads and times than did a HYAM (Fig. 3A, B and fig. S11). Corresponding SRAM structure changes during 0.1 Hz actuation to provide 8.5% stroke are shown in movie S1. Figure S12A shows that the equilibrium isometric contractile stress generated by a PEO-SO₃@CNT SRAM monotonically increases with increasing ethanol vapor concentration. In contrast, if the applied load is low and the change in sheath thickness is large, the SRAM first contracts until inter-coil contact occurs and then expands as inter-coil contact drives actuation (fig. S12C). Mandrel coiling greatly amplifies muscle stroke. A 70% tensile stroke was obtained for a humidity-driven cone-mandrel SRAM, and this SRAM provided faster contraction than cylindrical-mandrel SRAMs that were coiled and supercoiled (fig. S13).

The SRAMs provide advantages in contractile work capacity and maximum average contractile power (Fig. 3B, figs. S14-16 and S19, and Table S2), which is the maximum ratio of contractile work to actuation time. The maximum average contractile power output was 4.44 W/g for the ethanol-vapor-driven PEO-SO₃@CNT SRAM and 1.51 W/g for the corresponding HYAM. The load-optimized contractile work capacity and the maximum average power density of coiled SRAMs are higher than for coiled HYAMs at all applied loads for sorption-driven, electrothermal, and electrochemical actuation (Table S2). For loads maximizing equilibrium contractile work capacities, the SRAM-to-HYAM work capacity ratio was 1.84 for ethanol-vapor-driven PEO-SO₃@CNT muscles (Fig. 3B), 1.73 for electrothermally-driven PEO-SO₃@CNT muscles (Fig. 3D), and 2.15 for electrothermally-driven PU@CNT muscles (Fig. 4D), where PU is an elastomeric polyurethane (26). These SRAM-to-HYAM work

capacity ratios will approximately equal the ratio of energy conversion efficiencies for sorption-powered muscles in which the equilibrium gravimetric sorption of guest in SRAM sheath and in HYAM core are equal, and for thermal muscles in which the differences in heat lost during high-rate contractile work are negligible.

The SRAM-to-HYAM power density ratio (Table S2) is higher for ethanol-vapor-driven PEO-SO₃@CNT muscles (2.94) than for electrothermally-driven PEO-SO₃@CNT muscles (1.69) and PU@CNT muscles (2.06). This is likely because the power density ratio for the vapor-driven muscle is enhanced by both the larger equilibrium work capacity of the SRAM and the more rapid vapor absorption, and the latter diffusion-based enhancement term disappears when actuation is by electrothermally heating the CNT yarn.

Since the rate of cooling is faster for the SRAM than for the HYAM and the rate of cooling has the greatest impact on full cycle performance, the high-frequency work capacity during electrothermal actuation is much higher for a SRAM than a HYAM. The PEO-SO₃@CNT SRAMs electrothermally operated in air and in room-temperature water to produce 2.6 W/g (for 3.2% stroke at 9 Hz) and 9.0 W/g (for 5.5% stroke at 12 Hz), respectively, of full-cycle contractile power (fig. S15C-F), which is much higher than the typical contractile power of human natural muscle (0.05 W/g, 5). When operated in air, this SRAM muscle provided a stroke of 8.0% at 2 Hz, corresponding to a power density of 1.2 W/g. Movie S2 shows the electrothermal actuation of a coiled PEO-SO₃@CNT SRAM in water at 12 Hz to generate a 5% stroke and a full-cycle contractile power of 4.2 W/g.

We next predicted the stress dependence of tensile stroke and contractile work capacity for ethanol-powered actuation of coiled PEO-SO₃@CNT SRAMs and HYAMs (26, fig. S21). This analysis used the above theoretically-derived torsional strokes of twisted, non-coiled muscles, the relationship between torsional stroke (ΔT) and tensile stroke for non-contacting coils if muscle stiffnesses were constant, and the dependence of PEO-SO₃ modulus on ethanol absorption (fig. S4A). Remarkable agreement was obtained between theory and experiment for the stress dependence of equilibrium stroke and contractile work capacity without using a fitted parameter. The observed ratio of the maximum contractile work capacity of the SRAM to that of the HYAM is 1.70, which is close to the predicted 1.52 (fig. S22).

Electrochemical tensile actuation of coiled muscles

Electrochemically powered artificial muscles have key advantages over thermally powered muscles: (1) their efficiency is not limited by the Carnot efficiency and (2) they have a natural latching state, meaning that stroke can be maintained without the input of significant electrical energy. A conventional electrochemical CNT yarn muscle is a HYAM, wherein the yarn guest is the electrolyte.

A CNT@nylon6 SRAM was made by the process of Fig. 4A (right). Like for a process used to make coiled CNT yarns for energy harvesting (27), a stack of CNT sheets was formed into a cylinder (Fig. 4A, left). A nylon yarn was placed in the center of the cylinder. Initially, twist is inserted only into the CNT cylinder. However, once the CNT cylinder collapses to form a sheath on the nylon 6 yarn, torque automatically transfers from this sheath to the yarn, enabling the yarn to become fully coiled.

The electrolyte-filled CNT sheath of the SRAM and the electrolyte-filled volume of the HYAM provide electrochemical actuation because of volume changes produced by electrochemical double-layer injection of anions and cations. For the used electrolyte of 0.2 M tetrabutylammonium hexafluorophosphate ($\text{TBA} \cdot \text{PF}_6$) in propylene carbonate, the calculated van der Waals volume (28) of the TBA^+ cation ($\sim 293 \text{ \AA}^3$) is much larger than for the PF_6^- anion (69 \AA^3). Potential scans (Fig. 4B) for the SRAM and HYAM show that muscle contractions increase on both sides of the potential of zero charge and that the contraction is proportional to the volume of the injected ion. These contractions are largest for the SRAM.

Since the electrical energy required for actuation increases with increasing amount of electrochemically accessible CNTs, the contractile work per weight of CNT is an important performance metric. For slow square-wave switching at 10 mHz between 0 V to -3 V (Fig. 4C), the load-maximized contractile work capacity is slightly higher for the CNT@nylon6 SRAM (2.35 J/g) than for the CNT HYAM containing the same CNT weight per yarn length (2.01 J/g). However, for more practically applicable actuation rates (fig. S17), the ratios of SRAM to HYAM work capacities for similar tensile loads are much more impressive. For an applied square-wave frequency of ~ 0.3 Hz, this ratio is ~ 3.4 for all applied loads. At the highest measured frequency (5 Hz) and the highest applied load this ratio is 14.6. The electrochemical

actuation of a coiled CNT@nylon6 SRAM to provide 14.3% stroke at 0.25 Hz, while lifting a heavy load, is shown in movie S3.

Fig. 4D shows the frequency dependence of work capacity for a coiled CNT@nylon6 SRAM and a coiled CNT HYAM for square-wave voltages between 0 and -3 V. For 1 Hz cycle frequency, the tensile stroke, work per cycle, and average contractile power density for the SRAM were 4.7%, 0.99 J/g, and 1.98 W/g, as compared to 0.90%, 0.11 J/g, and 0.22 W/g for the HYAM. The high performance obtained for the SRAM at relatively high frequencies expands the application possibilities for electrochemical artificial muscles.

The contractile energy conversion efficiencies were obtained for optimized voltage scan rates between 0 and -2.7 V. This peak efficiency increased from 2.96% at 80 mV/s scan rate for the CNT yarn muscle to 4.26% at 130 mV/s scan rate for the SRAM (Fig. 4E). Using a higher potential scan rate for both muscles (200 mV/s, fig. S18), which increased stroke rates, provided a SRAM efficiency (3.8%) that is 2.7 times the HYAM efficiency (26).

Summary

Since the SRAM technology enables replacement of expensive CNT yarns with cheap commercially-available polymer yarns, whose sheath responds to targeted ambient variables, they are attractive for intelligent structures (29). Relevant for possible use in comfort adjusting clothing, SRAMs were knitted into a textile that increased porosity when exposed to moisture, and flat-coil SRAMs were demonstrated (figs. S23-S25). Analyte-powered sensors that intelligently respond in the body to open and close valves that release drugs in response to antigens (30) or biochemicals like glucose (31) are other possibilities. A CNT-free SRAM that linearly contracts with increasing glucose concentration was demonstrated (fig. S26), which could squeeze a pouch to release a drug (fig. S20).

The 5.2, 9.0, and 9.0 fold advantages at 1 Hz of the SRAM over the HYAM in electrochemical stroke, contractile work-per-cycle density, and average contractile power density (Fig. 4D) are important for electrically powered robotic devices in which stroke should be maintained without consuming significant electrical energy. Electrothermal PEO-SO₃@CNT SRAMs operated in air and in room-temperature water to produce 2.6 W/g (at 9 Hz) and 9.0 W/g (at 12 Hz) of full-cycle contractile power, respectively, compared with the

0.05 W/g typical of human muscle (5). SRAM performance and realizable low cost suggests their use for diverse applications, from fast, powerful muscles for humanoid robots and exoskeletons to intelligent comfort-adjusting clothing and drug delivery systems.

Acknowledgments: Support in the United States was from Air Force Office of Scientific Research Grant No. FA9550-18-1-0510 and FA9550-17-1-0328, Office of Naval Research Contract No. N68335-18-C-0368, National Science Foundation Grant No. CMMI-1661246, CMMI-1636306, and CMMI-1726435, Robert A. Welch Foundation Grant No. AT-0029, and the Louis Beecherl Jr. Endowed Chair. Australian support was from the Australian Research Council for a Centre of Excellence (CE140100012) and a DECRA Fellowship (DE12010517). Korean support was from the National Research Foundation of Korea for the Creative Research Initiative Center for Self-powered Actuation. Chinese support was from the Science and Technology Commission of Shanghai Municipality (16JC1400700).

Figures and Figures Captions:

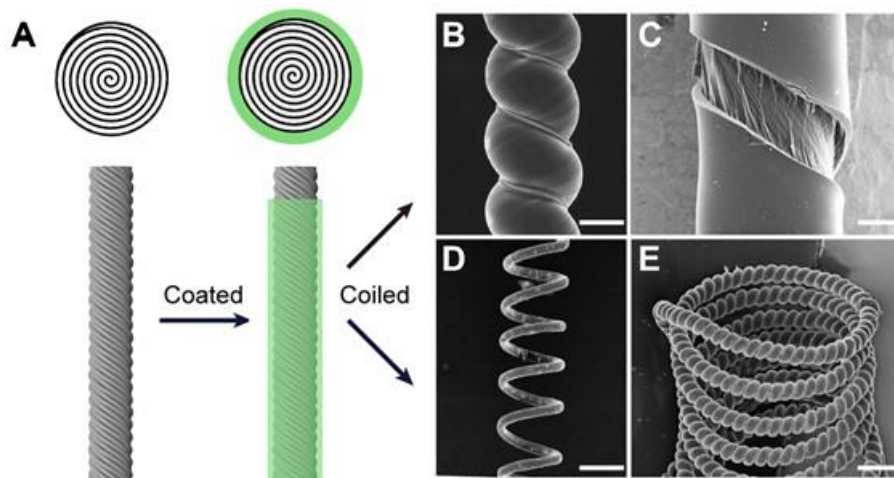


Fig. 1. Muscle fabrication and structure for torsional and tensile actuation. (A) Schematic lateral and cross-sectional views of a twisted CNT yarn and a SRAM, made by coating a twisted CNT yarn with a polymer sheath. SEM micrographs for PEO-SO₃@CNT muscles: (B) a SRAM made by self-coiling a sheath-coated twisted yarn, (C) the surface of a twisted SRAM, which was broken by untwisting in liquid N₂, showing the distinct boundary between sheath polymer and CNT core, (D) a mandrel-coiled twisted SRAM, and (E) a SRAM that was self-coiled and then supercoiled around a mandrel. The scale bars for (B)–(E) are 35, 15, 200, and 200 μm, respectively.

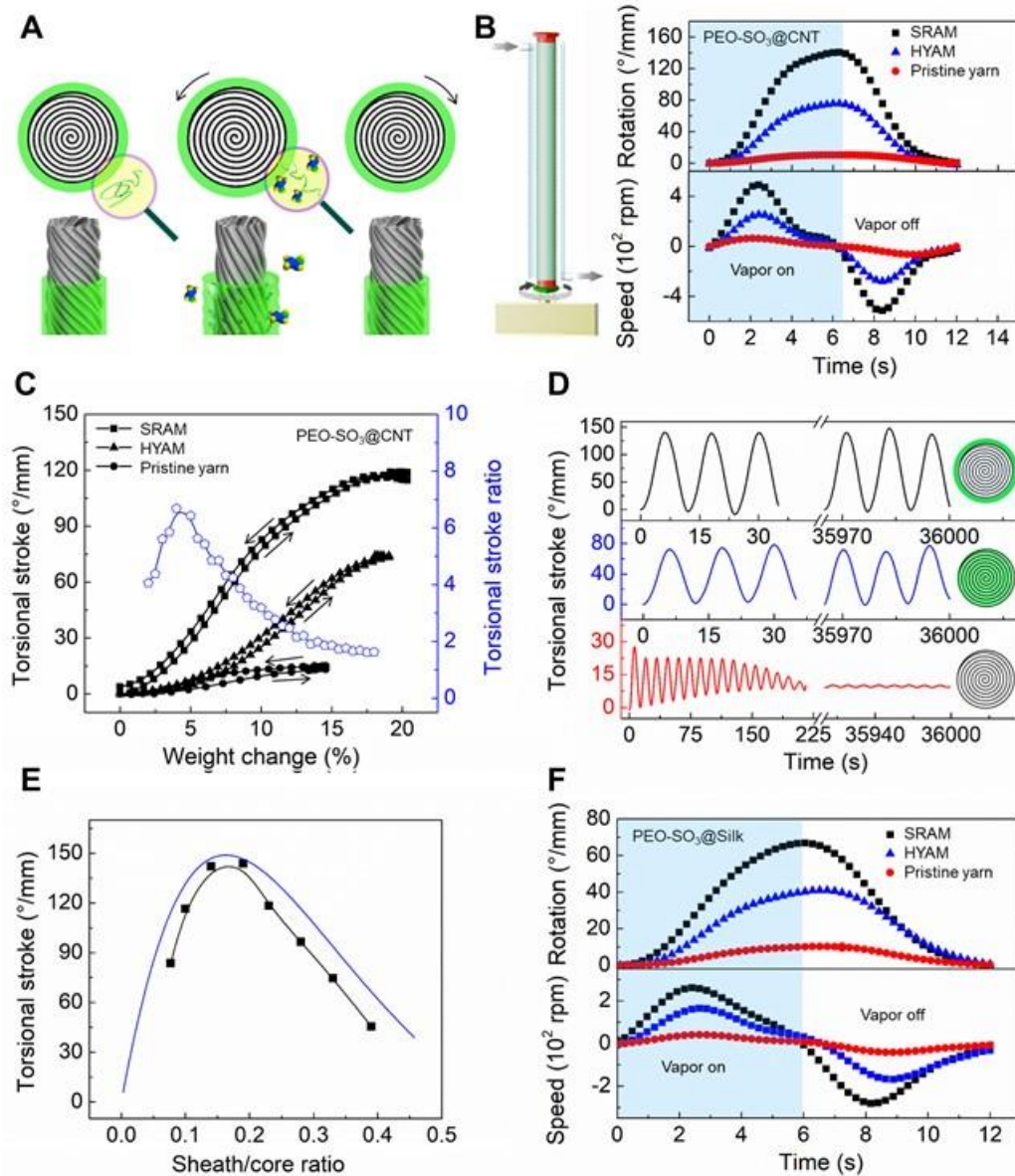


Fig. 2 Torsional actuation of twisted PEO-SO₃ sheath-run artificial muscles (SRAMs) and hybrid artificial muscles (HYAMs) driven by ethanol vapor. (A) Illustrations (left to right) of a PEO-SO₃ SRAM before vapor exposure and during vapor sorption and desorption, which cause yarn untwist and uptwist, respectively. (B) Illustration of vapor delivery to a muscle and plots of the time dependence of torsional stroke and rotation speed for one sorption/desorption cycle for a PEO-SO₃@CNT SRAM and HYAM and for a pristine CNT yarn. A 41- μ m-diameter pristine yarn, with 72 turns/cm of twist, was used for fabricating the 45- μ m-diameter SRAM and 50- μ m-diameter HYAM, which contained a 0.53 weight ratio of PEO-SO₃ to CNT. (C) Equilibrium torsional stroke vs. weight changes (black symbols) during ethanol absorption and desorption for the muscles of (B), and the SRAM-to-HYAM stroke ratio during ethanol absorption (blue pentagons). (D) Torsional stroke vs. time for the muscles of (B). (E) The observed (black squares) and predicted (blue line) dependence of torsional stroke on sheath/core ratio (SCR) for PEO-SO₃@CNT SRAMs (26). (F) Torsional stroke and rotation speed vs. time for a sorption/desorption cycle of a PEO-SO₃@silk SRAM and HYAM and a silk yarn. A 56- μ m-diameter silk yarn (with 5.7 turns/cm of twist) was used for fabricating the 90- μ m-diameter SRAM and HYAM, which weighed 0.48 mg/cm and contained a 0.27 weight ratio of PEO-SO₃ to silk.

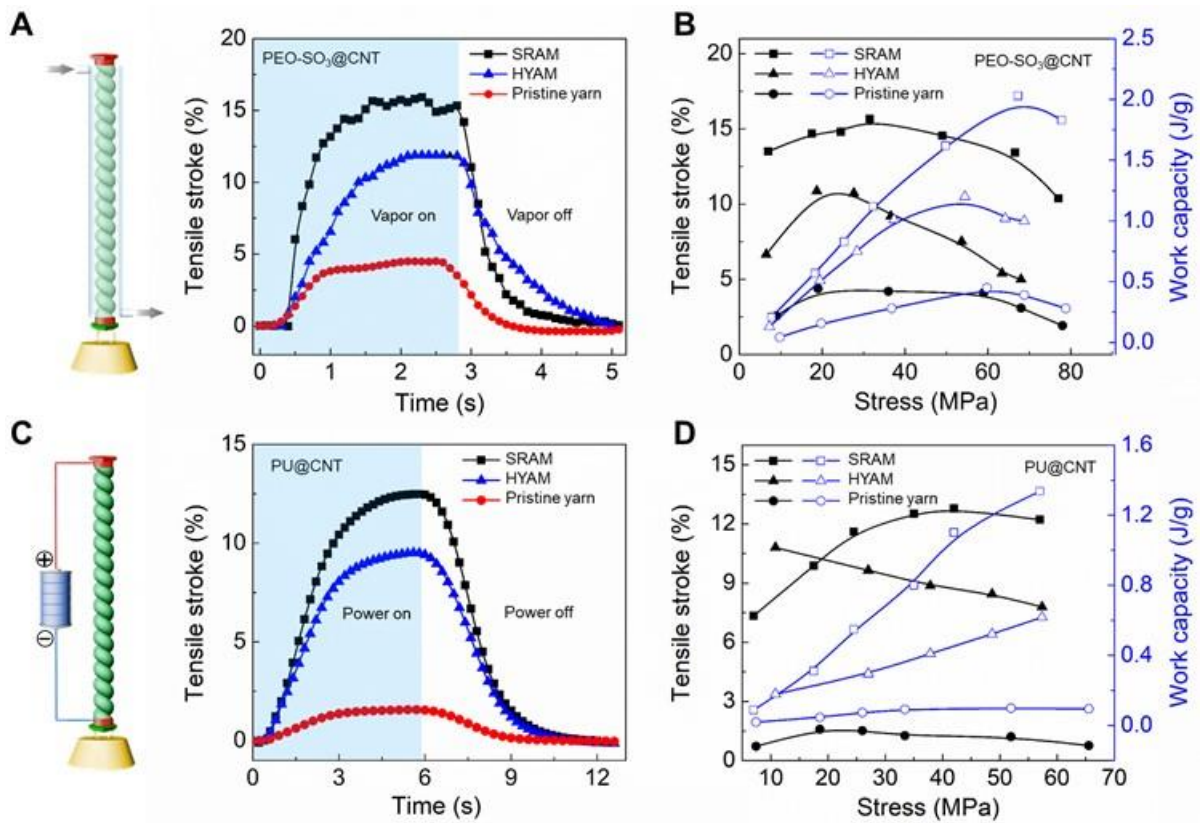


Fig. 3. Isobaric tensile actuation of self-coiled, sorption-powered and electrothermally-powered SRAMs, HYAMs, and pristine CNT yarns. (A) Tensile stroke vs. time for a PEO-SO₃@CNT SRAM and HYAM and a pristine yarn when actuated by ethanol absorption using the illustrated configuration and 33 MPa stress. Sorption was from a near-equilibrium ethanol concentration in dry air and desorption was by dynamic pumping. Before coiling, the diameters of the PEO-SO₃@CNT SRAM and HYAM and the pristine yarn were 43, 47, and 38 μm , respectively. (B) Tensile stroke and contractile work capacity vs. applied stress for the sorption-actuated muscles of (A). (C) The time dependence of tensile stroke for a PU@CNT SRAM and HYAM and a pristine CNT yarn when electrothermally actuated using the illustrated configuration, 42 MPa stress, and 0.25 W/cm power, which provided temperatures of 85, 93, 97°C, respectively. The device structure is shown on the left. Before coiling, the diameters of the PU@CNT SRAM and HYAM and the pristine yarn were 65, 71, and 51 μm , respectively. (D) Tensile stroke and contractile work capacity vs. applied stress for the electrothermally actuated yarns in (C).

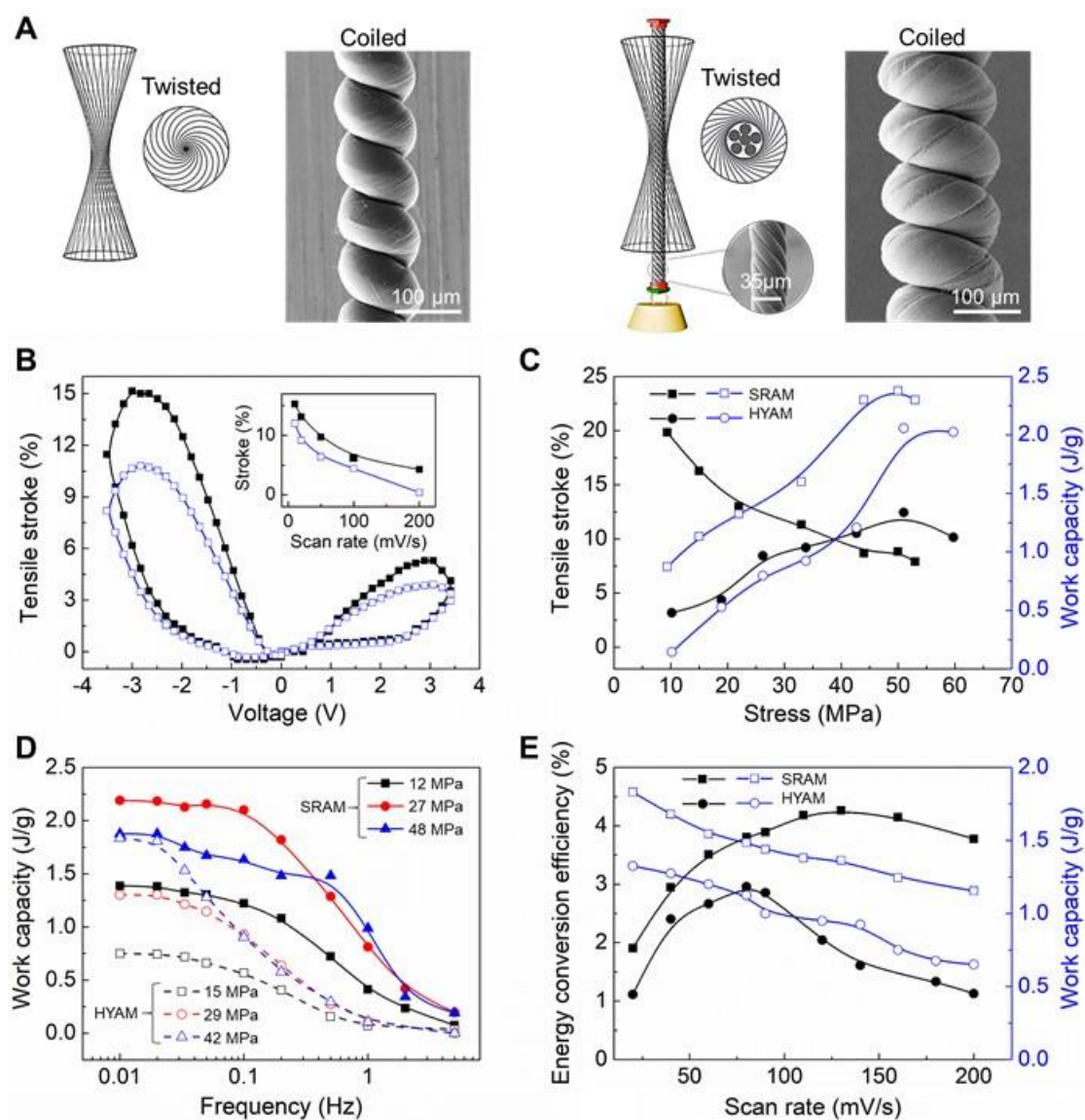


Fig. 4. Fabrication and electrochemical tensile actuation of coiled CNT@nylon6 SRAM and coiled CNT HYAM yarns in 0.2 M TBA·PF₆/PC electrolyte. (A) Illustration of cone spinning for fabricating CNT yarns (left) and its modification for making SRAM yarns (right). SEM micrographs of a coiled pristine yarn, a coiled CNT@nylon6 SRAM yarn, and a non-coiled nylon 6 yarn are shown. (B) Tensile stroke of the SRAM and HYAM during a cyclic voltammetry scan at 20 mV/s, under 22 MPa isobaric stress. Inset: Actuator stroke at this load for this muscle versus interelectrode voltage scan rate. (C) Tensile stroke and contractile work capacity vs. load when applying a 10 mHz square-wave voltage between 0 and -3 V. The spring indices of the 95- μm -diameter CNT@nylon6 SRAM and the 70- μm -diameter CNT HYAM were 0.88 and 0.56, respectively. (D) The frequency dependence of work capacity for a coiled CNT@nylon6 SRAM and a coiled CNT HYAM for square-wave voltages between 0 and -3 V. For 1 Hz cycle frequency, the tensile stroke, work-per-cycle, and average contractile power density for the SRAM at the highest loads were 4.7%, 0.99 J/g, and 1.98 W/g, compared to 0.90%, 0.11 J/g, and 0.22 W/g for the HYAM. (E) The scan rate dependence of work capacity and energy conversion efficiency for the SRAM and HYAM, using an applied stress of ~ 30 MPa for the SRAM and HYAM. For D and E, the spring indices of the 87- μm -diameter CNT@nylon6 SRAM and the 79- μm -diameter CNT HYAM were 0.97 and 0.67, respectively.

References and Notes

1. M. D. Lima, N. Li, M. Jung de Andrade, S. Fang, J. Oh, G. M. Spinks, M. E. Kozlov, C. S. Haines, D. Suh, J. Foroughi, S. Jeong Kim, Y. Chen, T. Ware, M. K. Shin, L. D. Machado, A. F. Fonseca, J. D. W. Madden, W. E. Voit, D. S. Galvão, R. H. Baughman, Electrically, chemically, and photonically powered torsional and tensile actuation of hybrid carbon nanotube yarn muscles. *Science* **338**, 928-932 (2012).
2. X. Gu, Q. Fan, F. Yang, L. Cai, N. Zhang, W. Zhou, W. Zhou, S. Xie, Hydro-actuation of hybrid carbon nanotube yarn muscles. *Nanoscale* **8**, 17881-17886 (2016).
3. Y. Sun, Y. Wang, C. Hua, Y. Ge, S. Hou, Y. Shang, A. Cao, Water-responsive helical graphene-oxide fibers incorporating a continuous carbon nanotube network. *Carbon* **132**, 394-400 (2018).
4. Y. Song, S. Zhou, K. Jin, J. Qiao, D. Li, C. Xu, D. Hu, J. Di, M. Li, Z. Zhang, Q. Li, Hierarchical carbon nanotube composite yarn muscles. *Nanoscale* **10**, 4077-4084 (2018).
5. S. M. Mirvakili and I. W. Hunter, Artificial muscles: Mechanisms, applications, and challenges. *Adv. Mater.* **30**, 1704407 (2017).
6. C. S. Haines, M. D. Lima, N. Li, G. M. Spinks, J. Foroughi, J. D. Madden, S. H. Kim, S. Fang, M. Jung de Andrade, F. Göktepe, O. Göktepe, S. M. Mirvakili, S. Naficy, X. Lepró, J. Oh, M. E. Kozlov, S. J. Kim, X. Xu, B. J. Swedlove, G. G. Wallace, R. H. Baughman, Artificial muscles from fishing line and sewing thread. *Science* **343**, 868-872 (2014).
7. S. H. Kim, M. D. Lima, M. E. Kozlov, C. S. Haines, G. M. Spinks, S. Aziz, C. Choi, H. J. Sim, X. Wang, H. Lu, D. Qian, J. D. W. Madden, R. H. Baughman, S. J. Kim, Harvesting temperature fluctuations as electrical energy using torsional and tensile polymer muscles. *Energy Environ. Sci.* **8**, 3336-3344 (2015).
8. S. Aziz, S. Naficy, J. Foroughi, H. R. Brown, G. M. Spinks, Characterization of torsional actuation in highly twisted yarns and fibres. *Polym. Test.* **46**, 88-97 (2015).
9. P. Zhang and G. Li, Healing-on-demand composites based on polymer artificial muscle. *Polymer* **64**, 29-38 (2015).
10. M. Hiraoka, K. Nakamura, H. Arase, K. Asai, Y. Kaneko, S. W. John, K. Tagashira, A. Omote, Power-efficient low-temperature woven coiled fibre actuator for wearable applications. *Sci. Rep.* **6**, 36358 (2016).
11. A. M. Swartz, D. R. Higuera Ruiz, H. P. Feigenbaum, M. W. Shafer, C. C. Browder, Experimental characterization and model predictions for twisted polymer actuators in free torsion. *Smart Mater. Struct.* **27**, 114002 (2018).
12. H. Cheng, Y. Hu, F. Zhao, Z. Dong, Y. Wang, N. Chen, Z. Zhang, L. Qu, Moisture activated torsional graphene fiber motor. *Adv. Mater.* **26**, 2909-2913 (2014).
13. J. Fan, G. Li, High performance and tunable artificial muscle based on two-way shape memory polymer. *RSC Adv.* **17**, 1127-1136 (2017).
14. S. M. Mirvakili, I. W. Hunter, Fast torsional artificial muscles from NiTi twisted yarns. *ACS Appl. Mater. Interfaces* **9**, 16321-16326 (2017).
15. J. Gong, H. Lin, J. W. C. Dunlop, J. Yuan, Hierarchically arranged helical fiber actuators derived from commercial cloth. *Adv. Mater.* **29**, 1605103 (2017).
16. C. Lamuta, S. Messelot, S. Tawfick, Theory of the tensile actuation of fiber reinforced coiled muscles. *Smart Mater. Struct.* **27**, 055018 (2018)

17. P. Chen, Y. Xu, S. He, X. Sun, S. Pan, J. Deng, D. Chen, H. Peng, Hierarchically arranged helical fibre actuators driven by solvents and vapours. *Nat. Nanotech.* **10**, 1077-1083 (2015).
18. J. Deng, Y. Xu, S. He, P. Chen, L. Bao, Y. Hu, B. Wang, X. Sun, H. Peng, Preparation of biomimetic hierarchically helical fiber actuators from carbon nanotubes. *Nat. Protoc.* **12**, 1349-1358 (2017).
19. W. Guo, C. Liu, F. Zhao, X. Sun, Z. Yang, T. Chen, X. Chen, L. Qiu, X. Hu, H. Peng, A novel electromechanical actuation mechanism of a carbon nanotube fiber. *Adv. Mater.* **24**, 5379–5384 (2012).
20. F. Meng, X. Zhang, R. Li, J. Zhao, X. Xuan, X. Wang, J. Zou, Q. Li, Electro-induced mechanical and thermal responses of carbon nanotube fibers. *Adv. Mater.* **26**, 2480-2485 (2014).
21. Ingi Agnarsson, A. Dhinojwala, V. Sahni, T. A. Blackledge, Spider silk as a novel high performance biomimetic muscle driven by humidity. *J. Exp. Biol.* **212**, 1990-1994 (2009).
22. J. Foroughi, G. M. Spinks, G. G. Wallace, J. Oh, M. E. Kozlov, S. Fang, T. Mirfakhrai, J. D. Madden, M. K. Shin and S. J. Kim, Torsional carbon nanotube artificial muscles. *Science* **334**, 494-497 (2011).
23. J. A. Lee, N. Li, C. S. Haines, K. J. Kim, X. Lepró, R. Ovalle-Robles, S. J. Kim, and R. H. Baughman, Electrochemically powered, energy-conserving carbon nanotube artificial muscles. *Adv. Mater.* **29**, 1700870 (2017).
24. S. H. Kim, C. H. Kwon, K. Park, T. J. Mun, X. Lepro, R. H. Baughman, G. M. Spinks, S. J. Kim, Bio-inspired, moisture-powered hybrid carbon nanotube yarn muscles. *Sci. Rep.* **6**, 23016 (2016).
25. M. D. Lima, S. Fang, X. Lepro, C. Lewis, R. Ovalle-Robles, J. Carretero-Gonzalez, E. Castillo-Martinez, M. E. Kozlov, J. Oh, N. Rawat, C. S. Haines, M. H. Haque, V. Aare, S. Stoughton, A. A. Zakhidov, R. H. Baughman, Biscrolling nanotube sheets and functional guests into yarns. *Science* **331**, 51-55 (2011).
26. Supplementary materials are available on Science Online.
27. S. H. Kim, C. S. Haines, N. Li, K. J. Kim, T. J. Mun, C. Choi, J. Di, Y. J. Oh, J. P. Oviedo, J. Bykova, S. Fang, N. Jiang, Z. Liu, R. Wang, P. Kumar, R. Qiao, S. Priya, K. Cho, M. Kim, M. S. Lucas, L. F. Drummy, B. Maruyama, D. Y. Lee, X. Lepró, E. Gao, D. Albarq, R. Ovalle-Robles, S. J. Kim, R. H. Baughman, Harvesting electrical energy from carbon nanotube yarn twist. *Science* **357**, 773-778 (2017).
28. M. Ue, A. Murakami, S. Nakamura, A convenient method to estimate ion size for electrolyte materials design. *J. Electrochem. Soc.* **149**, A1385-A1388 (2002).
29. M. A. McEvoy and N. Correll, Materials that couple sensing, actuation, computation, and communication. *Science* **347**, 1261689 (2015).
30. T. Miyata, N. Asami, T. Urugami, A reversibly antigen-responsive hydrogel. *Nature* **399**, 766-769 (1999).
31. J. Lee, S. Ko, C. H. Kwon, M. D. Lima, R. H. Baughman, S. J. Kim, Carbon nanotube yarn-based glucose sensing artificial muscle. *Small* **12**, 2085-2091 (2016).